DOI: 10.37190/ABB-02572-2024-03

Mechanical Analysis and Sensitivity Evaluation of PLA Scaffolds for Bone Tissue Repair Using FEA and Taguchi Experimental Design

Diego Vázquez[1], Luis Medina[2], Gabriela Martínez[2*]

[1]Escuela de Ingeniería Civil Mecánica, Facultad de Ciencias de la Ingeniería, Universidad Austral de Chile, Chile

[2]Instituto de Ingeniería Mecánica, Facultad de Ciencias de la Ingeniería, Universidad Austral de Chile, Chile

*Corresponding author: Gabriela Martínez, Instituto de Ingeniería Mecánica, Facultad de Ciencias de la Ingeniería, Universidad Austral de Chile, Chile, e-mail address: gabriela.martinez@uach.cl

Submitted: 27th December 2024

Accepted: 17th February 2025

Abstract:

Purpose

The design of three-dimensional scaffolds for bone regeneration poses challenges in balancing mechanical strength, porosity, and degradability. This study aims to optimize the geometric parameters of polylactic acid (PLA) scaffolds fabricated via 3D printing, focusing on pore size, porosity, and geometric configurations to enhance mechanical performance and biological functionality.

Methods

Two geometric configurations—orthogonal and offset orthogonal—were evaluated with pore sizes ranging from 400–1000 μm and porosities between 55–70%. Finite Element Analysis (FEA) in ANSYS Workbench was used to simulate mechanical behavior, while the Taguchi experimental design determined the optimal parameter combinations. Statistical analyses, including ANOVA, assessed the significance of each factor.

Results

The study identified a pore size of 400 μm as optimal for structural strength, while a porosity of 70% provided a balance between stability and cell growth. Orthogonal geometries distributed stress more uniformly, reducing critical stress concentrations compared to offset configurations. ANOVA revealed that pore size was the most significant factor, followed by porosity and geometry, achieving a model reliability of $R^2 = 98.42\%$.

Conclusions

The findings highlight the importance of geometric optimization for improving scaffold mechanical properties while maintaining biological functionality. This study offers a robust framework for designing patient-specific scaffolds tailored to bone tissue engineering applications.

Keywords:

Scaffolds, 3D printing, finite element method, experimental design, Taguchi method, sensitivity analysis, polylactic acid (PLA).

1. Introduction

Tissue engineering is an interdisciplinary field that has gained significant relevance in recent years due to its potential to provide solutions to complex medical problems, such as the regeneration of damaged tissues and the replacement of body parts. One of the major challenges

in regenerative medicine is the development of three-dimensional scaffolds capable of reproducing the properties and structure of natural tissue, ensuring effective integration into the human body and supporting the growth of new cells [13,27].

Scaffolds in tissue engineering act as temporary matrices that support cellular growth, enabling the regeneration of damaged or lost tissue. In the case of bone regeneration, an appropriate scaffold must not only provide mechanical support but also facilitate cellular infiltration and vascularization, which are critical for cell survival and proliferation. Bone regeneration scaffolds are particularly complex due to the mechanical and biological demands they must meet, such as strength, biocompatibility, and the ability to integrate with surrounding tissue [18,14]. Specifically, this integration can develop through mechanical adhesion, where the scaffold provides structural continuity with the host tissue, or through biological integration, which involves cellular interaction, bioactivity, and eventual remodeling by osteogenic cells. As bone tissue regenerates, the scaffold should gradually degrade, allowing the new tissue to replace it without leaving toxic residues in the body [11]. Achieving this balance between strength and degradation requires careful selection and optimization of scaffold materials and geometries.

The 3D printing technology has transformed scaffold fabrication, facilitating the creation of highly customized structures precisely tailored to meet the unique requirements of individual patients. Fused deposition modeling (FDM) has become one of the most used techniques in these applications [30,25]. This technique is also environmentally friendly, as it reduces material waste during production [32]. Unlike traditional manufacturing methods, 3D printing allows for the design of scaffolds with complex geometries and specific internal structures that align with the required mechanical and biological properties. Furthermore, this technology facilitates small-scale production, making it ideal for personalized medical devices that require individual adjustments for each patient [26].

Among the most used biomaterials in scaffold structures, polymers and their composites stand out due to their excellent manufacturing stability, biocompatibility, hypoallergenic response, and the ability to be produced with a wide range of porosities and pore sizes, allowing precise control of their mechanical properties [28]. Within this context, polylactic acid (PLA) has emerged as an ideal material for scaffold fabrication owing to its biodegradable and biocompatible properties, enabling its degradation within the body without eliciting adverse inflammatory responses [12]. Additionally, the degradation rate of PLA can be tuned through modifications in its molecular structure, allowing it to degrade at a rate compatible with the

bone healing process [15]. However, for PLA scaffolds to be effective, it is crucial to optimize their geometric parameters, including pore size, porosity, and structural configuration, as these factors directly affect permeability, stiffness, and the scaffold's load-bearing capacity [31].

The scaffold geometry and its structural properties play a critical role in its mechanical performance and its ability to promote tissue growing. Geometry determines the distribution of stress within the scaffold, which is essential for its stability and durability. Additionally, pore size and porosity influence permeability and the scaffold's ability to facilitate nutrient transport and oxygen flow, both of which are critical for cell survival in the scaffold environment. While increased porosity reduces mechanical properties, it is crucial for enabling cell growth and vascularization within the scaffold [34],[8], [17].

A significant discussion exists regarding the optimal porosity and pore size for scaffolds, primarily due to the heterogeneity of bone tissue depending on the anatomical location. Conventional guidelines recommend a porosity exceeding 50% for scaffold design [4]. Regarding pore size, a wide variability is observed, with studies indicating ranges between 100 μm and 1250 μm [21].

Conversely, a dilemma arises in the optimization of these parameters: increasing porosity and pore size can enhance nutrient flow but may simultaneously reduce the mechanical strength of the scaffold. This trade-off is particularly critical in applications such as bone regeneration, where scaffolds must bear specific loads while supporting cellular proliferation. Consequently, the selection of geometry, pore size, and porosity must balance permeability and strength, ensuring that the scaffold can withstand physiological loads without compromising its functionality in promoting tissue growth [31].

In this study, scaffold configurations are optimized using two key tools: structural analysis through the finite element method (FEA) and the Taguchi experimental design. FEA, a widely adopted engineering technique, simulates the mechanical behavior of structures under various loading conditions. This approach enables the prediction of scaffold responses to physiological loads, facilitating design optimization prior to fabrication [7]. On the other hand, the Taguchi experimental design is a statistical methodology used to optimize the design of complex systems using orthogonal arrays. In addition, a Taguchi L16 orthogonal array is employed to evaluate the influence of geometry, pore size, and porosity on the mechanical performance of PLA scaffolds. This technique allows the identification of optimal parameter combinations,

reducing experimentation time and costs, while providing a robust foundation for the design of patient-specific devices [14].

The geometric optimization of 3D-printed scaffolds is essential for their success in clinical applications, as an adequate design ensures the structural integrity of the scaffold while enhancing cellular proliferation and tissue integration at the regeneration site [11].

The creation of effective scaffolds for bone regeneration presents a challenge due to the requirement to balance factors such as stiffness, porosity, and degradability. This study aims to evaluate the mechanical behavior of PLA scaffolds fabricated with orthogonal and offset orthogonal configurations, varying pore size and porosity to identify the optimal combination of parameters. FEA simulations are conducted in ANSYS Workbench [3] to determine the maximum stresses experienced by the scaffolds under uniform displacement conditions, while the Taguchi design is employed to structure the experimental combinations of design parameters. Statistical techniques are applied to analyze the results and identify the variables with the greatest influence on stress outcomes.

2. Methodology

2.1 Materials and Mechanical Properties of PLA

Polylactic acid (PLA) was selected as the base material for scaffold fabrication due to its superior biodegradability, biocompatibility, and suitability for tissue engineering applications. PLA is a thermoplastic polymer synthesized from renewable resources, such as corn, further enhancing its sustainability for medical use. Its high mechanical strength and tunable degradation rate make it particularly well-suited for scaffolds designed to support tissue growth over a controlled timeframe before undergoing degradation and bioresorption within the body [12],[15].

The mechanical properties of PLA utilized in this study are detailed in Table 1. These properties were benchmarked against those of cortical and trabecular bone to ensure the material's capability to provide adequate mechanical support during the regeneration process, depending on the specific type of bone tissue being replaced.

Table 1. Mechanical properties of PLA [23], cortical bone [9], and trabecular bone [22].

Material	Cortical Bone	PLA	Trabecular Bone
Density [kg/m³]	1600–2000	1230	-
Strength [MPa]	71.56 ± 10.19	55	1.5–6.7
Young's Modulus [GPa]	18.2 ± 1.9	3.6	0.1–5.0

Poisson's Ratio	0.38 ± 0.02	0.38	-

2.2 Geometric Modeling of Scaffolds

Two geometric configurations of scaffolds were designed using Autodesk Inventor 2024© [5], specifically orthogonal and offset orthogonal configurations (see Figure 1). These configurations were developed based on research conducted by Tajbakhsh [29]. Each configuration offers distinct load distribution and resistance levels, making them suitable for evaluating the influence of geometric parameters on the mechanical performance of the scaffolds. The choice of these configurations was guided by previous research indicating that the arrangement of pores and the internal structure significantly influence the strength, stability, and biological functionality of scaffolds [26,10].

Based on the reviewed literature [4], [21], pore sizes ranging from 400 µm to 1000 µm and porosities exceeding 50% were selected.

The area and volume values of the scaffolds were directly obtained from Autodesk Inventor 2024©. The porosity percentage (PA) was calculated using Equation (1):

$$PA = \left(1 - \frac{V_{porosity}}{V_{solid}}\right) * 100\% \qquad (1)$$

Where:

- $V_{porosity}$: is the volume of the porous scaffold.
- V_{solid} : is the volume of the solid scaffold (the extruded geometry without internal porosity).

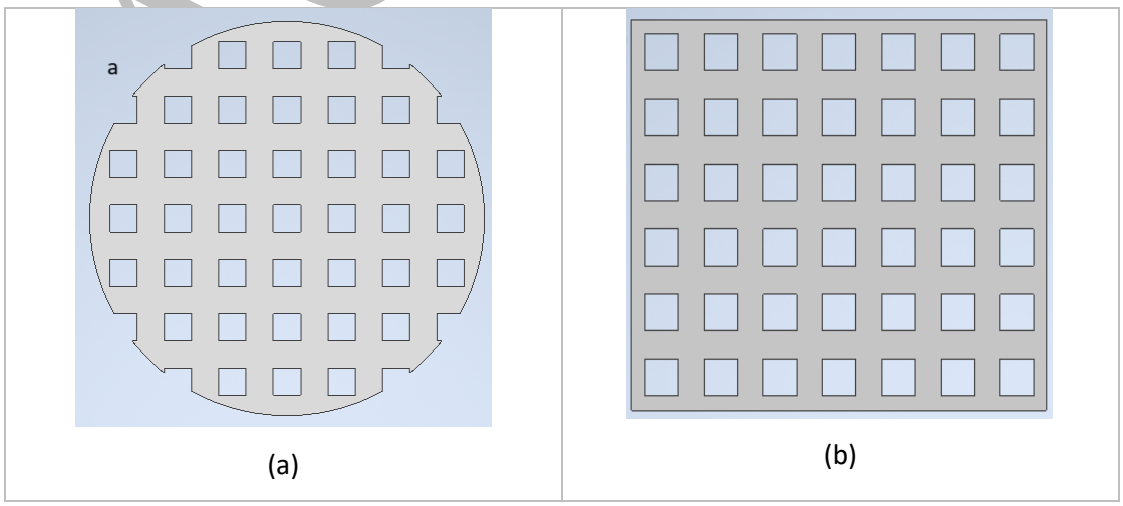

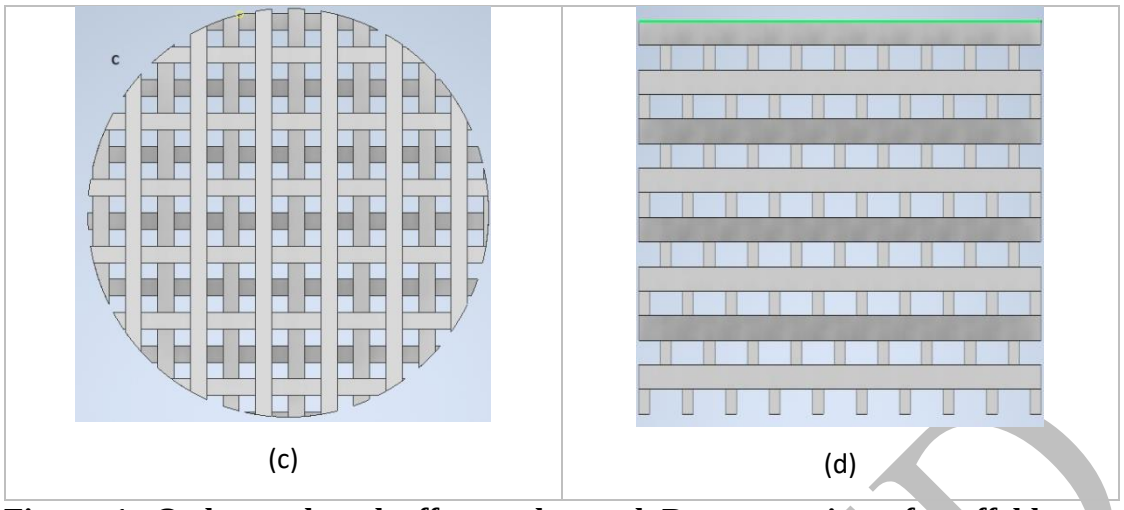

Figure 1. Orthogonal and offset orthogonal Representation of scaffold geometries. (a) Top view of orthogonal design, (b) lateral view of orthogonal design, (c) top view of offset orthogonal design, (d) lateral view of offset orthogonal design.

Three design factors were proposed for the evaluation: geometry, pore size, and porosity. The geometric configurations included orthogonal and offset orthogonal designs. Pore size levels were set at 400 μm, 600 μm, 800 μm, and 1000 μm, while porosity levels were defined as 55%, 60%, 65%, and 70%. The porosity was calculated using Equation (1). Table 2 lists the 32 resulting combinations, considering all factors and levels.

Table 2. Geometric characteristics of the scaffolds studied.

Scaffold	Pore Size (mm)	Volume (mm³)	Porosity (%)
Offset Orthogonal Scaffolds			
OD 1a	0.4	31.10	55
OD 1b		21.78	60
OD 1c		14.40	65
OD 1d		8.75	70
OD 2a	0.6	104.98	55
OD 2b		64.51	60
OD 2c		48.60	65
OD 2d		29.52	70
OD 3a	0.8	248.83	55
OD 3b		174.24	60
OD 3c		115.20	65
OD 3d		69.98	70
OD 4a	1.0	486.00	55
OD 4b		314.90	60
OD 4c		225.00	65
OD 4d		152.35	70
Orthogonal Scaffolds			
OR 1a	0.4	34.17	55
OR 1b		27.78	60
OR 1c		23.28	65

OR 1d		19.20	70
OR 2a	0.6	113.79	55
OR 2b		93.76	60
OR 2c		81.00	65
OR 2d		69.44	70
OR 3a	0.8	273.37	55
OR 3b		222.26	60
OR 3c		188.42	65
OR 3d		158.20	70
OR 4a	1.0	521.22	55
OR 4b		441.59	60
OR 4c		370.51	65
OR 4d		307.50	70

2.3 Finite Element Analysis (FEA)

Finite element analysis (FEA) was performed using the Static Structural tool in ANSYS Workbench© [3] to evaluate the mechanical behavior of the scaffolds under uniform tensile loads.

To simplify the model geometry and reduce computational costs, the scaffolds were represented as regular three-dimensional structures. In clinical applications, scaffolds often exhibit cylindrical or spherical shapes, which facilitate their insertion into bone and integration with surrounding tissue [11]. However, for this study, a representative cube was utilized for each combination of pore size and porosity percentage. This cube was created by replicating a unit cell nine times along the vertical axis and three times along the horizontal axes, ensuring that it accurately represented the scaffold structure's volume (Figure 2).

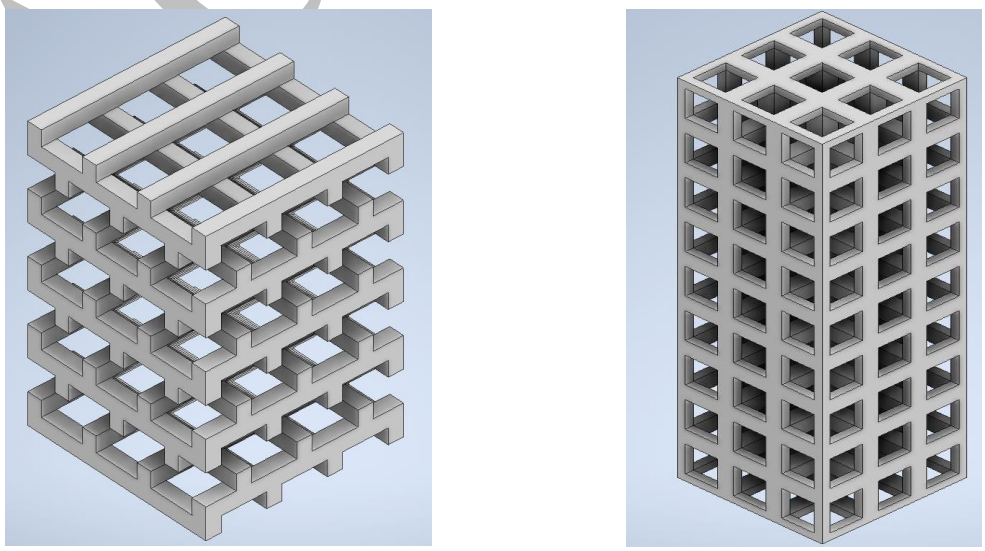

(a) (b)

Figure 2. Offset orthogonal structures (a) and orthogonal structures (b).

A mesh convergence analysis was performed to determine the element size at which further mesh refinement leads to minimal changes in the results. While refining the mesh reduces errors, it is important to acknowledge that the mesh always has some influence on the results, rather than becoming completely independent of mesh size. Tetrahedral meshes with varying element sizes were generated, progressively reducing the element size in each iteration. The convergence criterion was set as a relative variation in the maximum von Mises stress of less than 2% between consecutive iterations. To ensure a representative assessment, the offset orthogonal model (OD1c model) and the orthogonal model (OR1d model) were selected for the respective convergence analyses. Table 3 presents the iterations and the selected element sizes for each model. A progressive reduction of the elements throughout the mesh is observed until the desired relative error is achieved.

Table 3. Mesh Convergence for OR1d (Orthogonal) and OD1c (Offset Orthogonal) Geometries.

Mesh	Iteration	Element Size	Number of Elements	Max von Mises Stress (MPa)	Relative Error (%)
OR1d	1	0.2200	7,347	22.91	-
	2	0.1100	41,918	22.48	-1.9%
	3	0.0550	304,871	22.35	-0.6%
	4	0.0275	2,334,948	22.31	-0.2%
OD1c	1	0.2000	3,714	23.26	-
	2	0.1500	17,130	28.86	24.1%
	3	0.1425	18,212	28.19	-2.3%
	4	0.1375	22,287	28.11	-2.6%
	5	0.1250	29,479	28.47	1.3%
	6	0.1000	48,618	28.67	0.7%

To ensure standardized criteria and reproducibility across all geometries in the experiment, an element size was chosen to guarantee that at least two elements were present along the shortest edge of each geometry. For the OR1d geometry, iteration 2 (element size 0.11 mm) was chosen, as the shortest dimension of the geometry is 0.22 mm. Similarly, for the OD1c geometry, iteration 6 (element size 0.1 mm) was selected, corresponding to the shortest edge dimension of 0.2 mm. All geometries were meshed according to this criterion.

2.3.3 Boundary Conditions and Simulation

After defining the mesh, the necessary boundary conditions were applied to simulate a tensile test on the scaffolds. A displacement of 0.025 mm was imposed along the positive direction of

the "y" axis at the top of the scaffold, while the base was fixed using a clamping condition (Figure 3). These boundary conditions replicate the physiological environment in which scaffolds may experience tensile forces, simulating conditions found in both cortical and trabecular tissues. The applied displacement results in stress values that remain below the material's yield strength.

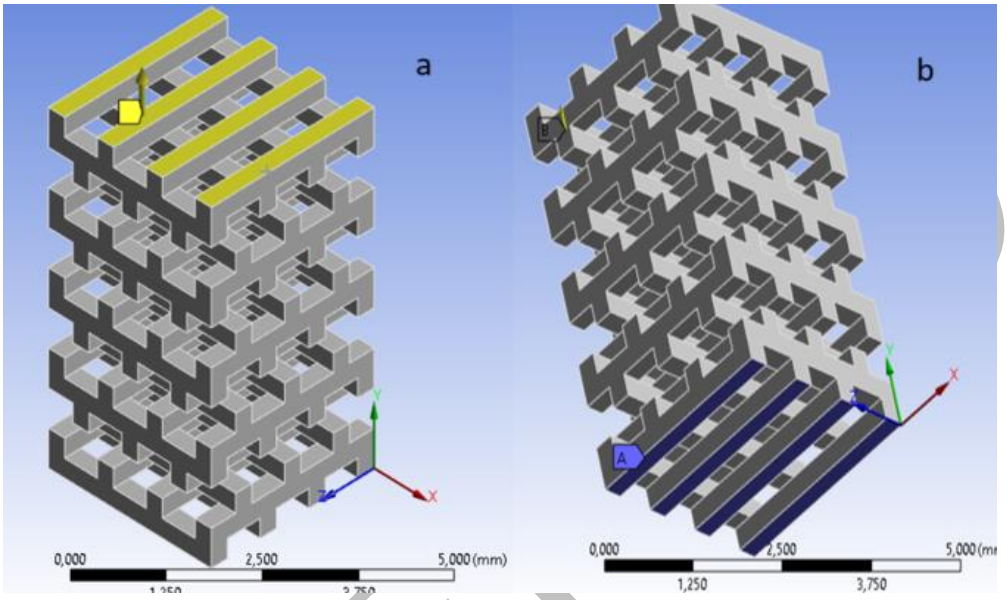

Figure 3. Boundary condition configuration for the simulation**.** a) Imposed displacement. b) Fixed support.

This configuration was applied to all 32 possible combinations of pore size, porosity, and geometry. The von Mises stress was selected as the output variable because it serves as a reliable metric for comparing the mechanical performance of the scaffolds to the properties of cortical or trabecular bone [12]. Two key response values were defined: the first is a "probe" control point, representing the von Mises stress measured as close as possible to the geometric center of the specimen to ensure a representative value. This location was designated as the control point. The second value corresponds to the maximum von Mises stress observed across the entire scaffold structure.

2.5 Parameter Influence

A combined methodology employing the Taguchi method and analysis of variance (ANOVA) was proposed to assess the sensitivity of design parameters influencing the mechanical behavior of scaffolds. This approach enables the identification of the optimal combination of factors and levels, maximizing desired responses while minimizing variability within a computational framework [16].

Three primary factors were considered for evaluation: pore size, porosity, and scaffold geometry. Pore size was assessed at four levels 400, 600, 800, and 1000 μm, while porosity was examined at levels of 55%, 60%, 65%, and 70%. The geometric configurations included two types: orthogonal (OR) and offset orthogonal (OD). These factors were selected due to their significant influence on the mechanical performance of scaffolds. Specifically, pore size and porosity directly affect the scaffold's strength and ability to support cellular growth, while geometry plays a crucial role in stress distribution within the structure. The responses analyzed included maximum von Mises stress, which indicates the scaffold's structural strength, and the stress at the midpoint (probe), which serves as a measure of stress distribution throughout the scaffold.

To reduce the number of required experiments, a Taguchi L16 orthogonal array was selected. This design reduces the number of experimental configurations from 32 to 16 while maintaining a statistical balance that facilitates the identification of main effects and potential interactions between factors. Subsequently, the signal-to-noise (S/N) ratio is calculated for each result to evaluate the proximity of the values to the desired targets and the variability in the data.

To identify the combination of levels that maximized the maximum von Mises stress and optimized the stress at the midpoint, the signal-to-noise (S/N) ratio was calculated using the formula for the "larger is better" criterion, as maximizing the maximum stress of the scaffolds is desirable.

Additionally, an analysis of variance (ANOVA) was performed on the signal-to-noise (S/N) ratio, enabling the determination of the statistical significance of the studied factors, the identification of the most influential factors, and the quantification of their relative contributions. Minitab® 21.4.1 [20] software was used for this evaluation. The general outline of the procedure is shown in Figure 4, which details each stage of the analysis.

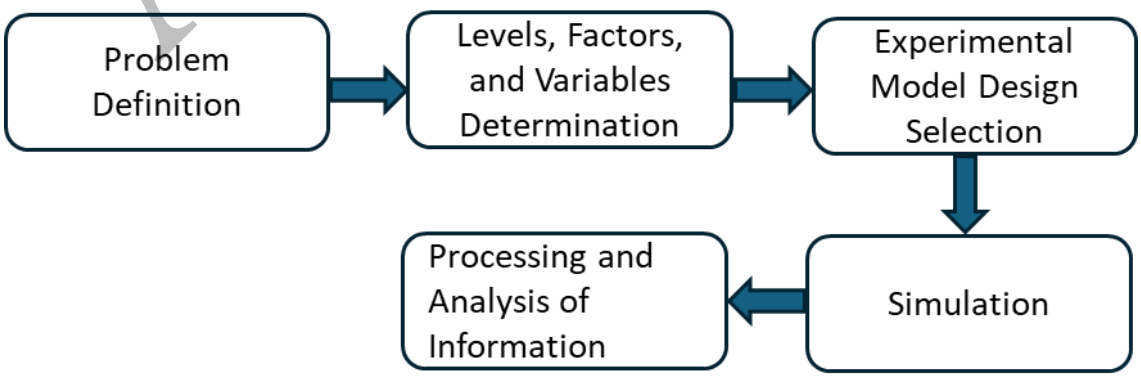

Figure 4. Procedural flowchart for sensitivity analysis.

3. Results and discussion

3.1 Simulation Results

Tensile simulations were conducted to analyze the mechanical behavior of PLA scaffolds in two primary geometric configurations: orthogonal and offset orthogonal. A displacement of 0.025 mm was applied to evaluate stress, with von Mises stress serving as the indicator of mechanical strength. Table 4 summarizes the results for all 32 combinations. The findings derived from these results provide insights into the influence of each design parameter.

Table 4. Results of the computational evaluation.

	Scaffold	Porosity (%)	Pore Size (mm)	Control Point (MPa)	Max von Mises Stress (MPa)
OD	1a	55	0.4	59.538	27.433
	1b	60	0.4	76.278	28.969
	1c	65	0.4	8.586	28 .670
	1d	70	0.4	88.379	29.540
	2a	55	0.6	42.305	19.198
	2b	60	0.6	55.541	19.369
	2c	65	0.6	66.191	19.063
	2d	70	0.6	79.187	19.687
	3a	55	0.8	51.362	14.527
	3b	60	0.8	60.163	14.488
	3c	65	0.8	73.606	14.297
	3d	70	0.8	82.208	14.771
	4a	55	1.0	41.076	11.391
	4b	60	1.0	50.198	11.604
	4c	65	1.0	58.885	11.438
	4d	70	1.0	58.122	12.014
	Scaffold	**Porosity (%)**	**Pore Size (mm)**	**Control Point (MPa)**	**Max von Mises Stress (MPa)**
OR	1a	55	0.4	14.198	21.457
	1b	60	0.4	14.663	22.230
	1c	65	0.4	15.840	22.250
	1d	70	0.4	16.802	22.480
	2a	55	0.6	10.518	14.310
	2b	60	0.6	10.730	16.120
	2c	65	0.6	10.994	14.830
	2d	70	0.6	11.034	15.270
	3a	55	0.8	7.222	10.731
	3b	60	0.8	79.639	11.167
	3c	65	0.8	83.426	11.291
	3d	70	0.8	62.359	11.250
	4a	55	1.0	62.359	8.636

4b	60	1.0	63.162	9.444
4c	65	1.0	66.523	9.065
4d	70	1.0	6.817	9.410

Following the computational analysis presented in Table 4, subsequent sections will detail the mechanical behavior of PLA scaffolds through comprehensive analysis and visualization. This methodological approach facilitates the understanding of design parameter effects on scaffold performance and stress distribution patterns.

Porosity Variation and Stress Behavior

For both geometric configurations, an incremental increase in von Mises stress is observed as porosity levels rise. This behavior is attributed to the reduction in the effective cross-sectional area, which results in elevated stress concentrations within the structure. The trend is consistently evident in both the stress measured at the control point and the maximum von Mises stress recorded across the scaffold.

Figure 5 provides a detailed illustration of the porosity variation in orthogonal and offset orthogonal geometries, maintaining a fixed pore size of 400 µm and porosities ranging from 55% to 70%, highlighting the impact on maximum von Mises stress. Similarly, Figure 6 depicts the relationship of these parameters to stress at the control point.

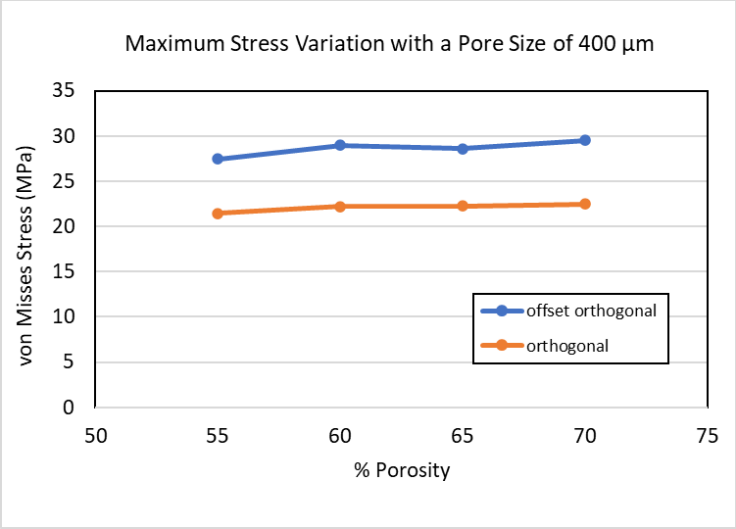

Figure 5. Maximum von Mises stress Variation for a pore size of 400 µm and different porosities. The behavior of orthogonal geometry and offset orthogonal geometry is illustrated.

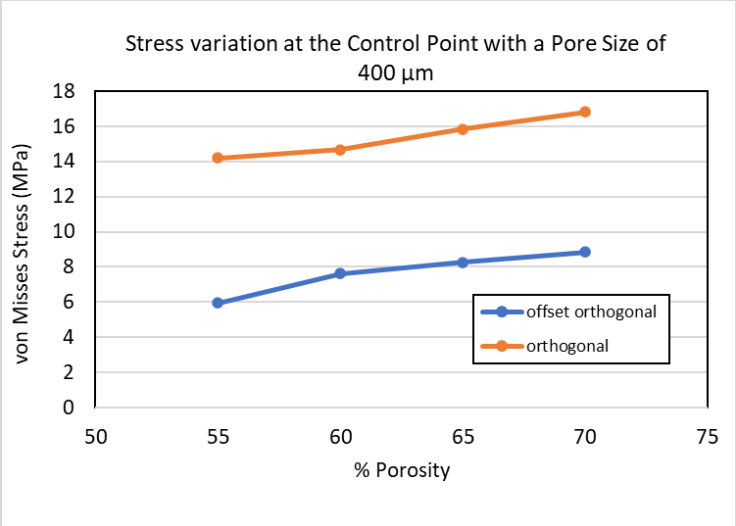

Figure 6. Stress Variation at the control point for a pore size of 400 µm and different porosities. The behavior of orthogonal geometry and offset orthogonal geometry is illustrated.

Figures 5 and 6 illustrate an increase in stress for both geometries as porosity increases. These findings are consistent with those experimentally obtained by Zhuo et al. [33] and Barzgar Torghabeh et al. [6], where compressive tests on square specimens with gyroid patterns and Kelvin geometries demonstrated that stress concentrations within the scaffold become more pronounced as porosity increases.

Pore Size Variation and Stress Behavior

Like porosity, both geometric configurations exhibit comparable trends. In this case, an increase in pore size results in a reduction in the maximum von Mises stresses. This behavior suggests that as pore size increases, the material density (in terms of the solid volume) decreases, thereby reducing the stresses the structure can support. Illustratively, Figure 7 demonstrates how, with a fixed porosity of 55%, varying the pore size from 400 µm to 1000 µm leads to a decrease in maximum stress for both orthogonal and offset orthogonal geometries.

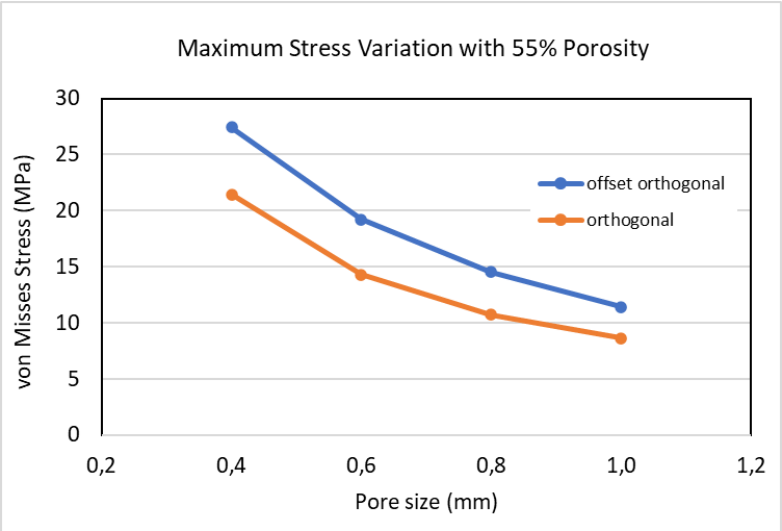

Figure 7. Maximum stress variation of for a fixed porosity of 55% and different pore sizes. The behavior of orthogonal geometry and offset orthogonal geometry is illustrated.

The Figure 8 shows the evolution of pore size (400 µm to 1000 µm) in relation to the stress measured at the control point. Both orthogonal and offset orthogonal geometries are evaluated with a fixed porosity of 55%.

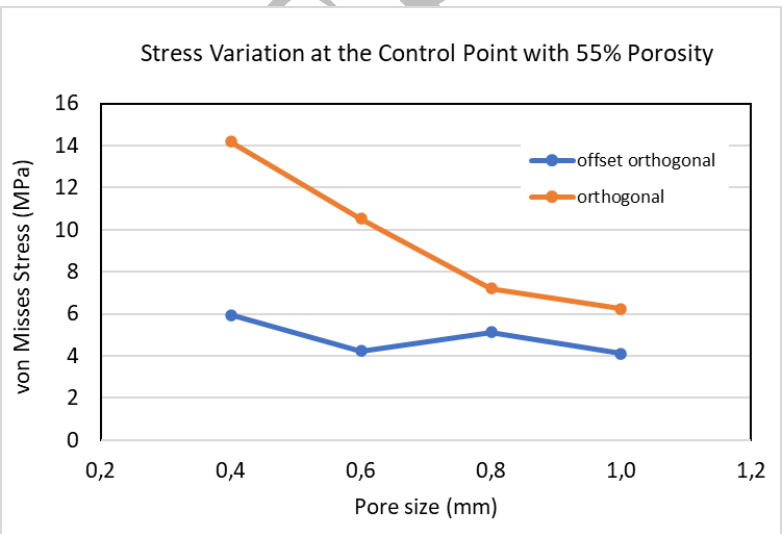

Figure 8. Stress variation at the control point for a fixed porosity of 55% and different pore sizes. The behavior of orthogonal geometry and offset orthogonal geometry is illustrated.

Both figures (Figure 7 and Figure 8) show a decrease in stress concentration as the effective cross-sectional area of the scaffold increases. This result is expected when scaling the specimen and is consistent with the tests conducted by Alizadeh-Osgouei et al. [2], where the mechanical properties of lattice-type structures subjected to experimental tensile tests exhibited similar behavior.

Effect of Geometry Type on Stress

Regarding the stress at the control point, the orthogonal geometry consistently exhibits higher stress values compared to the offset orthogonal geometry across all pore sizes and porosity levels. This suggests that the orthogonal structure distributes loads more efficiently, albeit with higher stress concentrations at certain points. Figure 9 illustrates this trend for all 32 scaffold configurations studied. The orthogonal and offset orthogonal geometries were extensively studied by Puppi et al. [24] and Serra et al. [26]. In both cases, the compressive modulus exhibited higher stiffness in orthogonal geometries compared to offset orthogonal ones. It can be inferred that the reduction in mechanical stability of offset geometries is attributed to the displaced disposition of the struts, which generates a combination of compressive and flexural stresses. In contrast, orthogonal geometries demonstrate higher average mechanical strength.

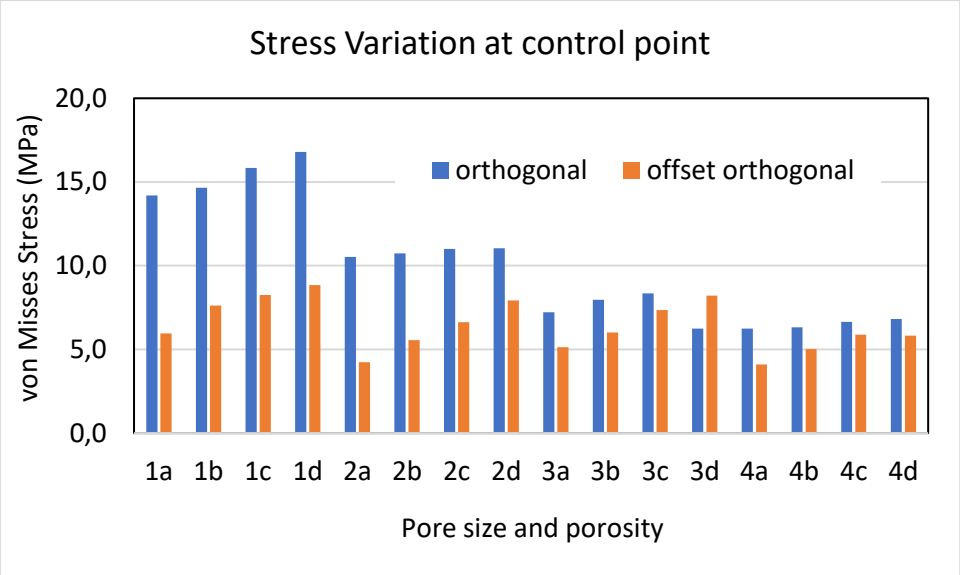

Figure 9. Stress variation at control points for orthogonal and offset orthogonal geometries.

Regarding the maximum von Mises stress, the offset orthogonal geometry exhibits higher stress values compared to orthogonal geometry. These stress concentrations under tensile loads result from geometric variations at the strut joints. The offset geometry has a higher number of geometric variations, leading to undesirable stress concentrations in applications that require uniform load distribution. Figure 10 illustrates this trend across the 32 scaffold configurations studied.

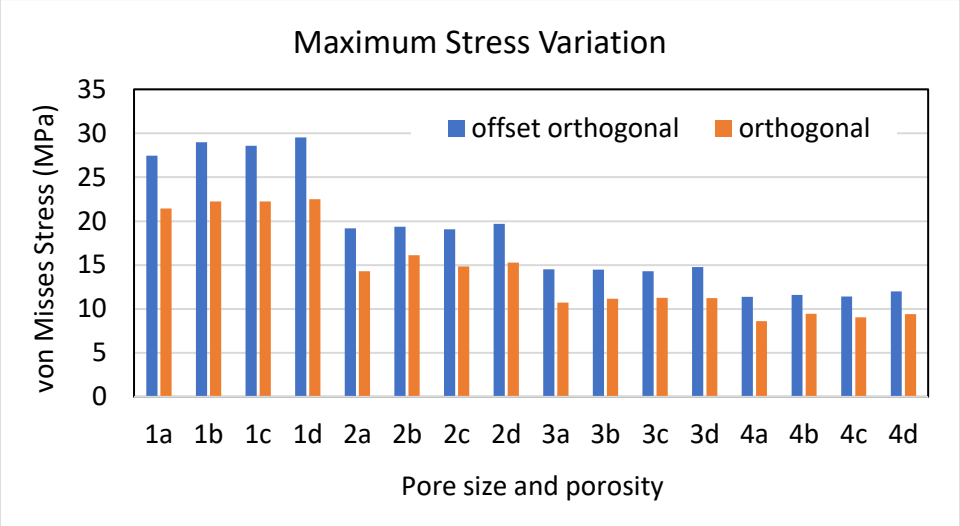

Figure 10. Variation of maximum stresses for orthogonal and offset orthogonal geometries.

A numerical-computational evaluation of the scaffolds was conducted, with a controlled displacement established as the loading condition. Based on this displacement, the structural response was analyzed in terms of maximum and average stress values. The results obtained were compared with previous experimental studies, where the loading condition was represented in terms of forces, and the responses were expressed as resistance modules. The comparison of results demonstrates a strong correlation with experimental studies, suggesting that numerical evaluation is a valid and effective tool, providing significant advantages in terms of cost and time efficiency.

3.2 Sensitivity of Pore Size, Porosity, and Geometry on Mechanical Behavior

The analysis presented in this section highlights the critical influence of pore size, porosity, and geometry on the mechanical performance of PLA scaffolds. The findings derived from Taguchi L16 experimental design (Table 5) and ANOVA analysis provide valuable insights into the structural behavior of scaffolds and their optimization for biomedical applications.

Table 5. Taguchi L16 Orthogonal Array

Scaffold	Pore Size (mm)	Porosity (%)	Geometry
OD 1a	0.4	55	Offset Orthogonal (OD)
OD 1b	0.4	60	Offset Orthogonal (OD)
OR 1c	0.4	65	Orthogonal (OR)
OR 1d	0.4	70	Orthogonal (OR)
OD 2a	0.6	55	Offset Orthogonal (OD)
OD 2b	0.6	60	Offset Orthogonal (OD)
OR 2c	0.6	65	Orthogonal (OR)
OR 2d	0.6	70	Orthogonal (OR)

OR 3a	0.8	55	Orthogonal (OR)
OR 3b	0.8	60	Orthogonal (OR)
OD 3c	0.8	65	Offset Orthogonal (OD)
OD 3d	0.8	70	Offset Orthogonal (OD)
OR 4a	1.0	55	Orthogonal (OR)
OR 4b	1.0	60	Orthogonal (OR)
OD 4c	1.0	65	Offset Orthogonal (OD)
OD 4d	1.0	70	Offset Orthogonal (OD)

The results clearly indicate that pore size is the most influential factor in the mechanical strength of the scaffold. As presented in Table 6, the highest delta value ($\Delta = 4.76$) among the main effects corresponds to pore size, confirming its dominant role in structural performance. The signal-to-noise (S/N) ratio plot (Figure 11) further supports this conclusion, displaying a pronounced gradient for pore size. This finding is consistent with previous studies [1], [19], where smaller pores have been associated with an increase in mechanical strength, attributed to a higher solid volume fraction, which enhances load-bearing capacity.

Porosity was identified as the second most significant factor in scaffold strength ($\Delta = 4.46$ in Table 6). The trend observed in Figure 11 indicates that as porosity increases, stress levels also rise, suggesting that higher porosity scaffolds experience greater stress concentrations due to the reduction in the effective cross-sectional area. This behavior aligns with previous research [31,34], which has demonstrated that while higher porosity enhances cell infiltration and nutrient diffusion, it also increases von Mises stress values, potentially compromising scaffold durability.

Although geometry exhibited a lower delta value ($\Delta = 3.80$ in Table 6) compared to pore size and porosity, its impact on stress distribution remains relevant. The orthogonal configuration was identified as the most favorable for optimizing von Mises stress distribution, as it reduces stress concentrations in critical regions.

Table 6. Summary of Main Effects for Signal-to-Noise (S/N) Ratios

Level	Pore Size	Porosity (%)	Geometry
1	20.41	15.27	15.86
2	17.27	16.64	19.66
3	17.71	19.39	-
4	15.65	19.74	-
Delta (Δ)	4.76	4.46	3.80

A better visualization is provided in Figure 11, which displays the main effects plot for signal-to-noise (S/N) ratios.

Figure 11. Main effects plots for S/N ratios.

The gradient displayed in the plot for the pore size factor shows that it is the most significant factor. Illustratively, if the goal is to maximize the response variable, the optimal combination involves a pore size of 400 µm, 70% porosity, and a fully orthogonal pattern.

To evaluate the influence of the parameters, an analysis of variance (ANOVA) was performed, establishing a minimum confidence level of 95%. A statistical significance level of 0.05 ($p = 0.05$) was applied to determine the influence of pore size, porosity, and geometry on the mechanical properties. The significance level was used to ensure that the observed differences were not due to random variation but rather reflected meaningful effects of the design parameters.

This analysis revealed p-values below 0.05 for all three factors (pore size, porosity, and geometry), showing for each factor significantly impacts the scaffold's strength (see Table 7). The model's R-squared value was 98.42%, suggesting that the model is reliable in explaining the variability of the results based on the factors considered.

Table 7. Variance Analysis (ANOVA) for S/N Ratios

Source	DF	Sum of Squares (SS)	Mean Square (MS)	F-Value	P-Value
Pore Size	3	46.912	15.6372	48.46	0.000018
Porosity Percentage	3	55.977	18.6590	57.82	0.000009
Geometry	1	57.755	57.7553	178.97	0.000001
Residual Error	8	2.582	0.3227	-	-
Total	15	163.22	-	-	-

Finally, the residual plots provide important evidence regarding the normality of the experimental data. In Figure 12a, the residuals closely follow the central line, indicating a

normal distribution. Figure 12b further illustrates how the residuals are distributed around the mean line, demonstrating that they are symmetrically spread above and below it. Additionally, the histogram in Figure 12c visually confirms this normal distribution pattern. Establishing that the residuals behave normally is crucial, as it validates the assumptions underlying our statistical analyses and enhances the reliability of our findings.

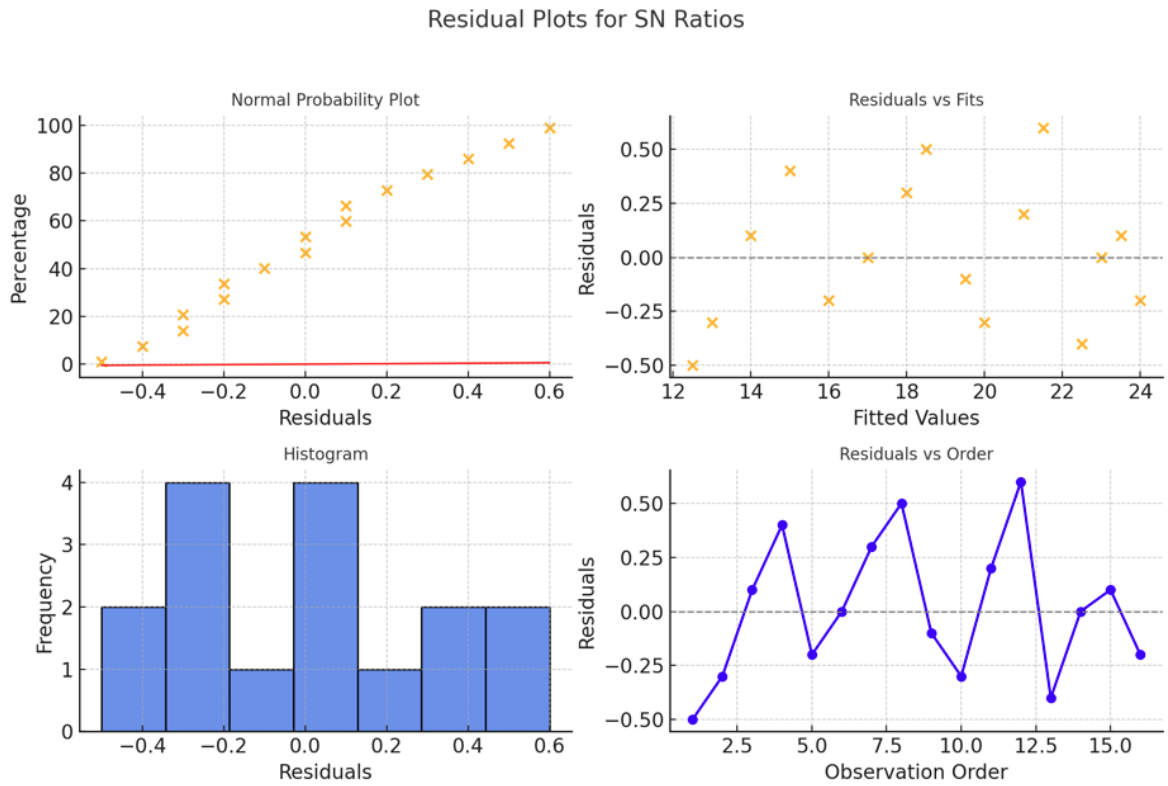

Figure 12. Residual plots for S/N ratios.

The residual analysis confirms the reliability of the experimental model and underscores the necessity of meeting statistical assumptions when evaluating scaffold performance. The normality of residuals supports the validity of the findings, ensuring that the conclusions drawn are statistically sound. This analysis provides a rigorous assessment of the data, offering insights that can inform future research and optimize scaffold design for bone regeneration applications.

Conclusions

Based on the bibliographic review conducted, it is evident that it is not possible to finally determine a specific geometry, pore size, and porosity percentage that would provide optimal conditions for osseointegration and vascularization in bone regeneration. The variability is due to numerous factors, including the patient's age, nutritional status, the location of the bone

defect, the scaffold manufacturing process, and the intrinsic characteristics of the materials used.

However, a design zone can be identified where encouraging results have been achieved regarding cell proliferation in *in vitro* scaffold assays. This zone involves a spectrum ranging from a pore size of 200 μm to 1000 μm and porosity percentages exceeding 50%, reaching up to 90% in selected cases.

From the mechanical response derived from the three factors evaluated in this study, the following conclusions can be drawn:

- Pore size was found to be the most critical factor influencing the strength of PLA scaffolds. A pore size of 400 μm was shown to be optimal for maximizing structural strength without compromising the scaffold's functionality, underscoring the importance of this parameter in optimizing structures for tissue engineering.
- The analysis revealed that a porosity of 70% provides an optimal balance between mechanical stability and the ability to promote cell growth. The results also confirm that as porosity increases, von Mises stress values increase, which must be carefully considered when designing scaffolds for load-bearing applications.
- The orthogonal geometry achieved a more uniform stress distribution compared to the offset orthogonal configuration, resulting in reduced stress concentrations at specific points. This suggests that, for tissue engineering applications, the orthogonal configuration may be more advantageous in terms of strength and structural stability.
- Statistical analysis confirmed the reliability of the model. ANOVA results showed p-values below 0.05 for all three parameters (pore size, porosity, and geometry), confirming their significant influence on mechanical performance. The model achieved a high R^2 value of 98.42%, indicating a strong predictive capability and reliability in explaining result variability.
- Comparison with experimental studies demonstrated a strong correlation, suggesting that numerical evaluation methods, such as FEA, are valid tools for scaffold design and optimization. The numerical approach provides significant advantages in cost and time efficiency compared to purely experimental methods.

The results of this study highlight the significance of geometric optimization in designing PLA scaffolds for bone regeneration. The optimal parameters identified—a pore size of 400 μm and a porosity of 70%—demonstrate a favorable balance between mechanical strength and biological functionality. Future research should explore additional materials beyond PLA, such as composites that may offer enhanced properties or degradation profiles. Investigating the long-term performance of these optimized scaffolds in vivo will be essential for validating their effectiveness in clinical applications. Moreover, integrating bioactive agents into the scaffold design could further improve cellular interactions and tissue regeneration outcomes. By addressing these areas, future studies can build upon these findings to develop more effective scaffolds tailored for specific tissue engineering needs.

Acknowledgments

The authors gratefully acknowledge the support provided by the Faculty of Engineering Sciences at the Universidad Austral de Chile. They also extend their gratitude to Minitab, LLC, for providing trial access to their software.

Statements

The authors declare that they have no conflicts of interest regarding the content presented in this article.

References

1. ABPEIKAR Z., MILAN PB., MORADI L., ASADPOUR S., *Influence of pore sizes in 3D-scaffolds on mechanical properties of scaffolds and survival, distribution, and proliferation of human chondrocytes*, Mech Adv Mater Struct., 2021, 29(26), 1-12, DOI: 10.1080/15376494.2021.1943077.
2. ALIZADEH-OSGOUEI M., LI Y., VAHID A., ATAEE A., WEN C., *High strength porous PLA gyroid scaffolds manufactured via fused deposition modeling for tissue-engineering applications*, Smart Mater Med., 2021, 2, 15-25, DOI: 10.1016/ j.smaim.2020.10.003.
3. ANSYS Workbench [Internet]. ANSYS, Inc. [cited 2024 Dec 27]. Available from: https://www.ansys.com.
4. ARABNEJAD S., JOHNSTON RB., PURA JA., SINGH B., TANZER M., PASINI D., *High-strength porous biomaterials for bone replacement: A strategy to assess the*

interplay between cell morphology, mechanical properties, bone ingrowth, and manufacturing constraints, Acta Biomater., 2016, 30, 345–356, DOI: 10.1016/ j.actbio.2015.10.048.

5. Autodesk Inventor 2024® [Internet]. Autodesk. [cited 2024 Dec 27].
6. BARZGAR TORGHABEH A., BARZGAR TORGHABEH I., KAFAEE RAZAVI M., *3D Printed PLA Porous Scaffolds with Engineered Cell Size and Porosity Promote the Effectiveness of the Kelvin Model for Bone Tissue Engineering*, Macromol Mater Eng., 2024 Aug 5, DOI: 10.1002/ mame.202400212.
7. BERGSMA JE., ROZEMA FR., BOS RR., BOERING G., *Bone reaction to biodegradable poly(L-lactide) implants: A long-term study in rats*, Biomaterials, 1995, 16(1), 25–31, DOI: 10.1016/0142-9612(95)91092-D.
8. BHARADWAZ A., JAYASURIYA AC., *Recent trends in the application of widely used natural and synthetic polymer nanocomposites in bone tissue regeneration*, Mater Sci Eng C, 2020, 110, 110698, DOI: 10.1016/j.msec.2020.110698.
9. CARTER DR., HAYES WC., *The compressive behavior of bone as a two-phase porous structure*, J Bone Joint Surg Am., 1977, 59(7), 954–962, DOI: 10.2106/JBJS.59.7.954.
10. CEA K., DONOSO M., SÉRANDOUR G., MARTÍNEZ G., ALEGRÍA L., *Evaluation of parameters in PLA and PCL scaffolds to be used in cartilaginous tissues*, Rev Mex Ing Biomed., 2021, 42(2), 149–159, DOI: 10.17488/RMIB.42.2.12.
11. CHEN Y., ZHANG X., PAN L., *Fabrication and application of biocompatible and biodegradable materials for bone tissue engineering*, Mater Sci Eng C, 2021, 124:112072, DOI: 10.1016/j.msec.2021.112072.
12. FARAH S., ANDERSON DG., LANGER R., *Physical and mechanical properties of PLA, and their functions in widespread applications: A comprehensive review*, Adv Drug Deliv Rev., 2016, 107, 367–392, DOI: 10.1016/j.addr.2016.06.018.
13. FRANCIS AP., AUGUSTUS AR., CHANDRAMOHAN S., BHAT SA., PRIYA VV., RAJAGOPALAN R., *A review on biomaterials-based scaffold: An emerging tool for bone tissue engineering*, Mater Today Commun., 2023, 34: 105124, DOI:10.1016/j.mtcomm.2022.105124.
14. GERMAIN L., TREMBLAY N., LABBÉ R., *Engineering of tissue scaffolds for skin and bone regeneration*, J Biomed Mater Res Part A, 2018, 106(7), 1845–1857, DOI: 10.1002/jbm.a.36283.
15. GRÉMARE A., GUDURIC V., BAREILLE R., HEROGUEZ V., LATOUR S., L'HEUREUX N., et al., *Characterization of poly-lactic acid (PLA) scaffolds for bone*

tissue engineering, J Biomater Sci Polym Ed., 2018, 29(9), 1008–1023, DOI: 10.1080/09205063.2018.1511554.

16. HERNÁNDEZ A., REYES R., SÁNCHEZ E., RODRÍGUEZ-EVORA M., DELGADO A., ÉVORA C., *Optimization of scaffolds for tissue engineering through the use of the Taguchi method*, J Tissue Eng Regen Med., 2015, 9(5), 626–636, DOI: 10.1002/ term.1874.
17. KIRILLOVA A., YEAZEL TR., ASHEGHALI D., PETERSEN SR., DORT S., GALL K., et al., *Fabrication of biomedical scaffolds using biodegradable polymers*, Chem Rev, 2021, 121(18), 11238–11304, DOI: 10.1021/ acs.chemrev.0C00744.
18. LANGER R., VACANTI JP., Tissue engineering, Science, 1993. 260(5110), 920–926, DOI: 10.1126/science.8493529.
19. LIU Q., WEI F., COATHUP M., SHEN W., WU D., *Effect of porosity and pore shape on the mechanical and biological properties of additively manufactured bone scaffolds*, Adv Healthc Mater., 2023 Sep 9, DOI: 10.1002/ adhm.202301111.
20. Minitab® 21.4.1 [Internet]. State College, PA: Minitab, LLC; [cited 2024 Dec 27]. Available from: https://www.minitab.com.
21. MOHAMMADI H., SEPANTAFAR M., MUHAMAD N., BAKAR SULONG A., *How does scaffold porosity conduct bone tissue regeneration?*, Adv Eng Mater., 2021, 23(6), 2100463, DOI: 10.1002/ adem.202100463.
22. MORGAN EF., UNNIKRISNAN GU., HUSSEIN AI., *Bone mechanical properties in healthy and diseased states*, Annu Rev Biomed Eng., 2018, 20, 119–143, DOI: 10.1146/ annurev-bioeng-071516-045113.
23. PARRADO-AGUDELO JZ., NARVÁEZ-TOVAR C., *Mechanical characterization of polylactic acid, polycaprolactone and Lay-Fomm 40 parts manufactured by fused deposition modeling, as a function of the printing parameters*, Iteckne. 2019, 16(2), 111–117, DOI: 10.17488/ Iteckne.16.2.12.
24. PUPPI D., MOTA C., GAZZARRI M., DINUCCI D., GLORIA A., MYRZABEKOVA M., AMBROSIO L., CHIELLINI F., *Additive manufacturing of wet-spun polymeric scaffolds for bone tissue engineering*, Biomed Microdevices, 2012 Dec, 14(6),1115-27, DOI: 10.1007/S10544-012-9677-0.
25. SENATOV FS., NIAZA KV., ZADOROZHNYY MY., MAKSIMKIN AV., KALOSHKIN SD., ESTRIN YZ., *Mechanical properties and shape memory effect of 3D-printed PLA-based porous scaffolds*, J Mech Behav Biomed Mater., 2016, 57, 139–148, DOI:10.1016/j.jmbbm.2015.11.036.

26. SERRA T., MATEOS-TIMONEDA MA., PLANELL JA., NAVARRO M., *Fabrication of PLA-based scaffolds using 3D printing*, J Biomed Mater Res Part A, 2013, 101(5), 1580–1590, DOI: 10.1002/jbm.a.34479.
27. SHICK T., ABDUL KADIR A., NGADIMAN N., MAHARAM A., *A review of biomaterials scaffold fabrication in additive manufacturing for tissue engineering*, J Bioact Compat Polym., 2019, 34(6), 415–435, DOI:10.1177/0883911519877426.
28. SUAMTE L., TIRKEY A., BARMAN J., BABU PJ., *Various manufacturing methods and ideal properties of scaffolds for tissue engineering applications*, Smart Mater Manuf., 2023, 1:100011, DOI: 10.1016/j.smmf.2022.100011.
29. TAJBAKHSH S., HAJIALI F., *A comprehensive study on the fabrication and properties of biocomposites of poly(lactic acid)/ceramics for bone tissue engineering*, Mater Sci Eng C, 2017, 70, 897–912, DOI: 10.1016/ j.msec.2016.09.008.
30. TYLER B., GULLOTTI D., MANGRAVITI A., UTSUKI T., BREM H., *Polylactic acid (PLA) controlled delivery carriers for biomedical applications*, Adv Drug Delivery Rev., 2016, 107, 163–175, DOI:10.1016/j.addr.2016.06.018.
31. UPADHYAY RK., SRIKAR R., SINGH J., MISHRA R., BALANI K., *Mechanical characterization of scaffolds for bone tissue engineering applications*, J Mech Behav Biomed Mater., 2016, 61, 451–465. DOI: 10.1016/j.jmbbm.2016.02.013.
32. WU GH., HSU SH., *Review: Polymeric-based 3D printing for tissue engineering*, J Med Biol Eng., 2015, 35(3), 285–292, DOI:10.1007/s40846-015-0039-7.
33. XU L., ZHUO EM., SARASINI F., RAZAVI N., *Quasi-static behavior of 3D printed lattice structures of various scales*, Procedia Struct Integr., 2021, 33, 578-85, DOI: 10.1016/ j.prostr.2021.10.064.
34. ZHEN W., YAO Z., JIANG X., WANG J., ZHANG Y., *Role of the porous structure of the bioceramic scaffolds in bone tissue engineering*, Nat Precedings, 2010, 5. DOI: 10.1038/NPRE.2010.4141.1.